Welding Research

Sponsored by the Welding Research Council of the Engineering Foundation

WRC

SUPPLEMENT TO THE WELDING JOURNAL, NOVEMBER 1970

Stress Corrosion Characteristics of Maraging Steel Weldments in Air and Pentaborane

Hydrogen embrittlement plays a major role in failure associated with stress corrosion cracking, and delayed weldment failure in air is associated with a cathodic hydrogen reaction as the source for hydrogen embrittlement

BY S. M. TOY AND A. PHILLIPS

ABSTRACT. The characteristics of the stress corrosion cracking of 18 Ni maraging steel weldments in air and pentaborane were identified by electron microscopy, electron microprobe, scanning electron microscopy, and by the use of the neodymium hydrogen detector system.

Electron fractographs of partial-through-thickness fracture toughness samples revealed the weld fracture to be primarily a quasi-cleavage type. The quasi-cleavage facets contained a herringbone with an included angle of approximately 100 to 110 deg depending on the line of sight position. These orientation lines were associated with thin martensite platelets in the massive martensite subgrains. Hydrogen was found to emanate from similar type martensite orientation locations. The austenite islands in the cored grain boundary encircling the martensite phase was observed to be cleaved.

A mechanism is postulated that hydrogen builds up in the retained austenite in the weld. The combination of local stress and hydrogen is necessary to transformation of the retained austenite into an H_2-embrittled martensite. Fracture then occurs along the preferred martensite or orientation directions observed.

Electron microprobe analysis indicated Ti and Fe segregated in the weld area; Ni, Co, and Mo concentration remained uniform. Methods recommended for reducing the stress corrosion susceptibility of these materials were based on our present knowledge of these phenomena.

S. M. TOY is with Douglas Aircraft Co., McDonnell Douglas Corp., Long Beach, Calif., and A. PHILLIPS is with McDonnell Douglas Aeronautics Co., Santa Monica, Calif.

Paper presented at the AWS National Fall Meeting held in Baltimore, Md., during October 5-8, 1970.

Introduction

The high strength 18 Ni maraging steels used in the aircraft and missile industry are susceptible to delayed failure in air and pantaborane (B_5H_9) in the welded condition. Both 250 grade and 300 grade 18 Ni maraging steel weldments failed when tested in air and pentaborane, but not in a vacuum. The base metals did not fail under the fracture toughness test matrix condition reported by Taketani.[1] He did find a homogenizing heat treatment of the welded steel at 1,800° F was beneficial.

The purpose of this investigation was to identify salient microstructural features responsible for the stress corrosion susceptibility of the maraging steel weldments, and also to identify them by their different H_2 emission characteristics. This could provide a classic example of how such information could be used not only to help explain hydrogen's role in the embrittlement of maraging steels, but also for its effect on other high strength aircraft steels.

Delayed failure of the 18 Ni maraging steel weldments in air is believed to be associated with an electrochemical mechanism. It is not known whether the maraging steel failures in pentaborane are associated with a chemical or electrochemical hydrogen embrittlement mechanism.

The characteristics of the specimens showing delayed failure of 18 Ni maraging steel weldments in air and pentaborane were identified by electron microscopy, electron microprobe, scanning electron microscopy, and by the use of the neodymium hydrogen detector system.

The neodymium hydrogen detector system was used to determine the emanation and distribution of hydrogen in the weld. It was based on the reaction of hydrogen with neodymium to form a metal hydride. The neodymium film is optically transparent so that the microstructure can be related to the neodymium hydride reaction site.

Experimental Procedure

Material Preparation

Fracture toughness specimens were fabricated from "as received" VASCO-MAX commercially annealed 250 grade

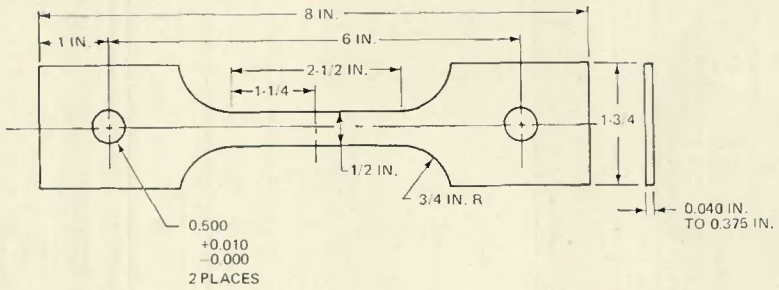

Fig. 1—Fracture toughness specimen

18 Ni and 300 grade 18 Ni maraging steel beveled sheet strips (24 × 4 × 1/8 in.) welded in the longitudinal direction by gas tungsten-arc welding with a modified 300 W grade filler metal high in titanium (see Table 1 for chemical compositions). The welded coupons 1.75 × 8 × 0.10 in. were machine welded into pin-loaded tensile specimens according to ASTM Standard E8–61T—Fig. 1.

Specimens were identified by two numbers:

1. A sequence number corresponding to slices from the test panel from right to left.

2. Test panel number.

An Elox notch 0.021 × 0.010 in. was formed 0.005 in. deep in the center of the weld area. The fracture toughness specimen was then aged 3 hr at 900° F (482° C in air) and then notch fatigued to form an 0.074 in. long starter crack (deflections of 0.300–0.25 in. were used). A Krouse flexual machine for flat sheets (3,500 cmp) was used to produce the crack length of 0.074 inch (approximately 6,000 to 13,000 cycles were required). These partial—through-thickness crack (PTC) tensile specimens were then loaded in a creep tensile tester to a K_{1i}/K_{1c} ratio equal to 90% where K_{1i} is the initial stress intensity or point determined by mechanical tensile tests at which catastrophic failure occurs.[2]

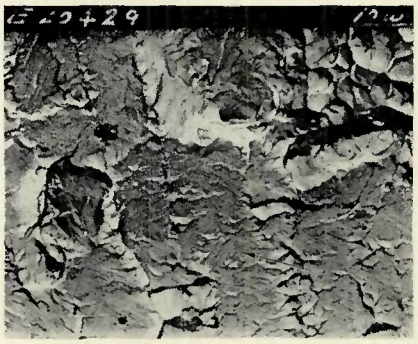

Fig. 3—Specimen 14 showing delayed failure fracture mode in quasi-cleavage (sustained load at 204 ksi failed after 93.6 hr in air)

Fig. 4—Specimen 36 showing flat cleavage facets of austenite island (dark grey triangular area). X10,000 (reduced 41% in reproduction)

Results and Discussion

Stress Corrosion Susceptibility in Air

Sustained Load Tests. Several sustained load tests on 250 grade Ni maraging steel weldments were run in air independently of those reported by Taketani (see Table 2). Specimen 1–5 failed in 210 hr and specimen 2–5 did not fail in 415 hr. Specimen 2–5 was unloaded and broken in a tensile machine at 243,000 psi. Fractographic examinations were conducted on these test specimens and compared to representative samples selected from the Taketani test group.[1]

Fractography Studies. The fractured surfaces of representative PTC specimens that failed in air were replicated by the plastic-carbon technique and examined by electron microscopy. Electron fractographs revealed the 250 grade Ni specimen 1–5 surface morphology was more than one-half quasi-cleavage

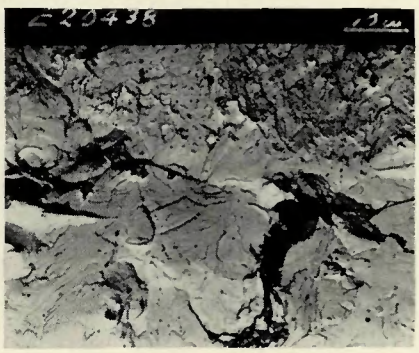

Fig. 5—Specimen 12 (250 Grade 18 Ni) showing pre-fatigue quasi-cleavage crack transition from top to bottom (failed in Pentaborane in seconds)

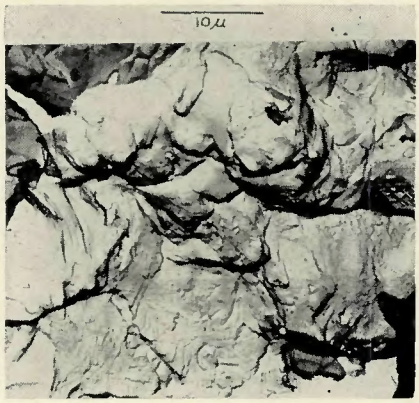

Fig. 2—Specimen 2-5 shows quasi-cleavage area broken under mechanical tension (no failure observed after 40 hr in air)

with the remainder dimple rupture. Specimen 2–5 showed a small flaw growth region which was quasi-cleavage; the remainder of the specimen fractured mechanically—Fig. 2.

The stretched zone in the overload region observed by Taketani in the base metal (specimen 2–4) was different from the fracture found in the welded samples. In the overload region of specimen 2–5, the fracture was observed to be a fixed mode of quasi-cleavage and dimple rupture (micro-void coalescence). These brittle fractures have quasi-cleavage facets containing a herringbone pattern with an included angle of approximately 100–110 deg, de-

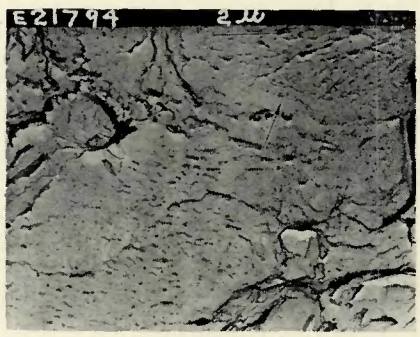

Fig. 6—Specimen 31 (300 Grade 18 Ni) showing morphology of precipitates in martensite phase (failed in Pentaborane in seconds)

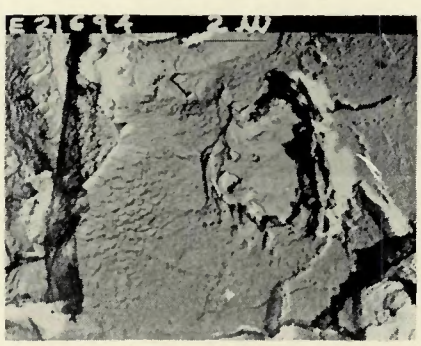

Fig. 7—Specimen 31 (300 Grade 18 Ni) showing austenite island with large, angular precipitates and finer precipitate in martensite matrix

Table 1—Chemical Composition of Maraging Steel, %

Grade	Heat no.	C	Si	Mn	S	P	Mo	Co	Ni	Al	Ti	B	Zr	Ca
250	04040	0.01	0.01	0.02	0.005	0.004	4.88	8.01	18.41	0.13	0.45	0.002	0.012	0.05
300	04862	0.012	0.01	0.03	0.004	0.003	4.93	9.32	18.36	0.14	0.69	0.004	0.011	0.05
300[a]	V-248	0.02	0.04	0.02	0.006	0.005	4.80	9.73	17.50	0.10	1.06	0.003	0.015	0.02

[a] Filler metal.

Table 2—18 Ni Maraging Steel Sustained Load Test Matrix

	Welded 250 grade maraging steel			Welded 300 grade maraging steel		
Test media	As-welded and aged[a]	1,800° F for 16 hr and aged	250 grade base metal	As-welded and aged	1,800° F for 16 hr and aged	300 grade base metal
Vacuum	NF[b]—672 hr (No growth)	—	—	NF[b]—110 hr (No growth)	—	—
Air	F[b]—48 hr	NF[b]—480 hr (Flaw growth)	NF[b]—405 hr (Flaw growth)	F[b]—24 hr	NF[b]—271 hr (Not exam for growth)	NF[b]—148 hr (No growth)
Pentaborane	F[b]—sec	F[b]—408 hr	NF[b]—672 hr (No growth)	F[b]—sec	F[b]—24 hr	NF[b]—672 hr (No growth)

[a] Aged—900° F for 3 hr.
[b] NF—no failures, F—failed.

pending on the line of sight position.

Similar surface morphology was observed on specimen 14 at the prefatigue quasi-cleavage transition zone taken from the Taketani test series. Figure 3 is an enlargement of the quasi-cleavage zone. It appears that the direction of crack propagation is parallel to the herringbone pattern lines. A similar cleavage pattern was found on 300 grade Ni maraging steel weldment, specimen 35. These lines are apparently associated with the martensite laths in the massive martensite subgrains. Hydrogen was found to emanate from similar type martensite patterns.

The austenite islands in the "cored" grain boundaries encircling the martensite phase appear to be cleaved. An examination of the fractured surface revealed it to be a flat cleavage facet—Fig. 4. A step-wise quasi-cleavage mode of the martensite can also be observed. The brittle behavior of austenite islands is associated with hydrogen and strain induced transformation of austenite to martensite. Hydrogen was found to emanate from the austenite islands. A similar mode of failure in air for the 300 grade 18 Ni steel weldments was also evident.

Stress Corrosion Susceptibility in Pentaborane

Fractography Studies. Fractography examination of 250 grade 18 Ni weldment (specimen 12) which failed in pentaborane, revealed practically a complete quasi-cleavage surface morphology—Fig. 5 This mode of cracking was typical of other PTC specimens which failed in pentaborane. The flat cleavage facets have similar herringbone morphology found for the specimens which failed in air.

The 18 Ni maraging steel weldments failed rapidly in pentaborane. The 300 grade 18 Ni weldments appeared to be more susceptible than the 250 grade 18 Ni weldments. The homogenization heat treatment of the weldments increased the 250 grade weldment resistance to failure more effectively than the 300 grade (see Table 1).

The base metals did not fail under the test conditions cited.

Fractography of Etched Surfaces. The introduction of hydrogen into the 18 Ni maraging steel weldments in air is by an electrochemical reaction. The stress corosion cracking mechanism is supported by the sustained load test evidence that the weldments do not fail in vacuum but do in air. It can be assumed that the air provides moisture for the electrolyte necessary for an electrochemical reaction to proceed and supply the hydrogen. The 18 N maraging steel weldment becomes susceptible by a thermal sensitization process. If the thermal embrittlement was inherent in the material, it would have failed in vacuum.

The nonsusceptibility of the base metal to stress corrosion cracking may be a function of the protective film that forms on the fracture surface prior to the exposure of the test environment. The improvement of the resistance to failure of the weldments by a homogenization heat treatment further emphasizes the need to identify the microstructural features that sensitize the steel weldments.

The introduction of hydrogen into

Table 3—Electron Diffraction Pattern from Extraction Replica Surface of 300 Grade 18 Ni Weld Pattern

Extraction replica of specimen 31 (Unknown)		TiC[a]		Fe_2Mo_4C[b]		σ FeMo[c]	
I/Io	d(Å)	I/Io	d(Å)	I/Io	d(Å)	I/Io	d(Å)
M	2.90	—	—	—	3.20	—	—
S	2.10	100	2.18	100	2.12	60	2.08
M	1.48	50	1.54	60	1.43	10	1.44
U	1.12	—	—	60	1.11	60	1.10
W	1.05	—	1.09	100	1.07	70	1.02
W	0.96	30	0.97	—	—	60	0.97

[a] ASTM X-ray powder data file card 6-0614.
[b] ASTM X-ray powder data file card 3-0980.
[c] ASTM X-ray powder data file card 9-290.

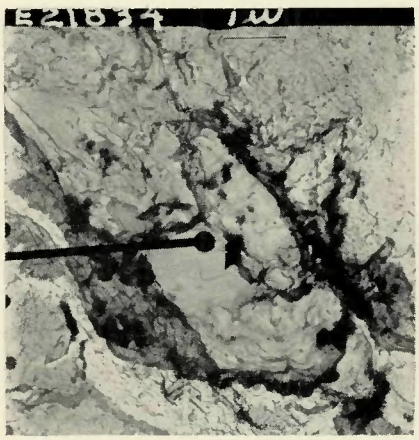

Fig. 8—Specimen 31 electron diffraction area examined in austenite island

Fig. 9—Specimen 31 electron diffraction area examined in martensite matrix

Table 4—Electron Diffraction Pattern from Extraction Replica Surface of 300 Grade 18 Ni Weld Fracture

Extraction replica of specimen 31 (Unknown)		TiC[a]		TiN[b]		τ—Ti_2S[c]	
I/Io	d(Å)	I/Io	d(Å)	I/Io	d(Å)	I/Io	d(Å)
	2.92	50	2(1.54)	56	2(1.50)	50	2(1.54)
S	2.68, 2.70		—		—	20	2.69
	2.19		—		—	100	2.22
	2.14	100	2.18	100	2.12		—
	1.37		—		—	60	1.38
S	1.33, 1.34	30	1.31				
	1.27	10	1.26	26	1.28	50	1.30
	1.20, 1.21		—	16	1.22	50	1.21
	0.99	5	1.00	7	1.06	70	1.01
	0.90	30	0.97	22	0.95	20	0.95

[a] ASTM X-ray powder data file card 6-0614.
[b] ASTM X-ray powder data file card 0642.
[c] ASTM X-ray powder data file card 11-664.

these local microstructural features of the Ni maraging steels, when exposed to pentaborane has not been directly established. It is assumed that the hydrogen could be supplied by either a chemical reaction or by an electrochemical reaction. The fracture surface of 300 grade 18 Ni (specimen 31) was etched with Fry's etchant for 8 sec to accentuate the local microstructural phase. Figure 6 shows the fine precipitate in the martensite phase lines in a herringbone fashion similar to the pattern in the martensite flat cleavage facets and where hydrogen emanation was observed.

Figure 7 is an electron fractograph of a typical austenite island revealing the large angular precipitates and other finer particles. The large angular particles are probably titanium compounds. Particles with similar morphology have been identified as Ti (C, N).[3]

Electron diffraction of one of the fine particles extracted from another austenite island indicated it to be either $Fe_3 Mo_3 C$ or σ-FeMo compound (see Table 3 and Fig. 8). The presence of a complex metal carbide in the austenite is generally associated with stress corrosion cracking of austenitic stainless steels.[4]

Figure 9 shows an electron diffraction pattern taken from extractive replica of the martensite fractured surface region of the 300 grade 18 Ni weldment specimen 31. The electron diffraction data give indirect evidence of Ti (C, N) and τ-Ti_2S in the region (see Table 4). This is a reasonable interpretation based on examined electron diffraction data reported by other investigators.[3, 5]

Microstructural Investigation. The fracture profile of the 250 grade 18 Ni weldment (specimen 12) which failed in pentaborane was examined. Fracture failure mode is quasi-cleavage through the martensite laths with cleavage across the austenite islands—Fig. 10.

Electron microprobe analysis of this fracture profile section was made. The back scattering electron micrograph shown in Fig. 11 indicates heavy elements in the light region and light elements in the dark regions of the fracture profile. X-ray scanning (Fig. 12) indicates specific weld areas have higher concentrations of titanium associated with them. The opposite effect was found for iron—Fig. 13. The percentage of iron varied from 49 to 66%. Ni, Co, and Mo concentrations remained uniform.

Figure 14 is an electron micrograph of 300 grade 18 Ni weldment (specimen 52B) which failed in air and 250 grade 18 Ni base metal next to the weldment (specimen 12).

The absence of austenite islands and the cored cast structure of the original weld are observed. The local precipitation appears to be general.

Electron micrographs of the 250 grade

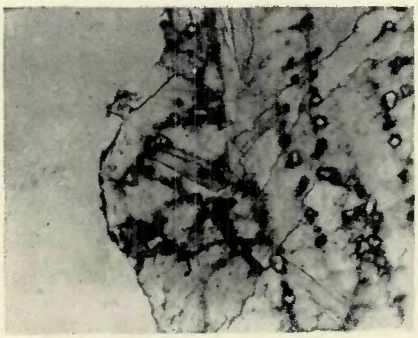

Fig. 10—Specimen 12 (250 Grade 18 Ni) fracture profile failed in Pentaborane). X940 (reduced 50% on reproduction)

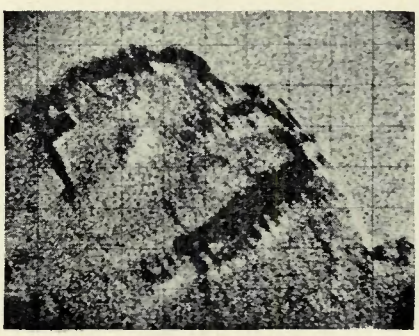

Fig. 11—Specimen 12 showing back scattering electron micrograph

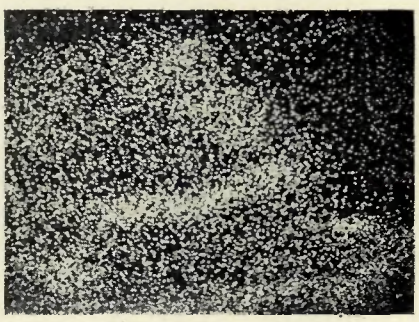

Fig. 12—Specimen 12 X-ray scan for titanium

Fig. 13—Specimen 12 X-ray scan for iron

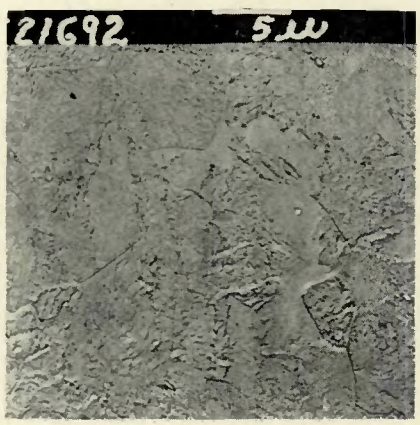

Fig. 14—Specimen 12 (250 Grade 18 Ni) base metal microstructure

Fig. 15—Specimen 2-6, 2-7 (250 grade 18 Ni) showing distribtuion of Ti (C,N) precipitate in austenite island

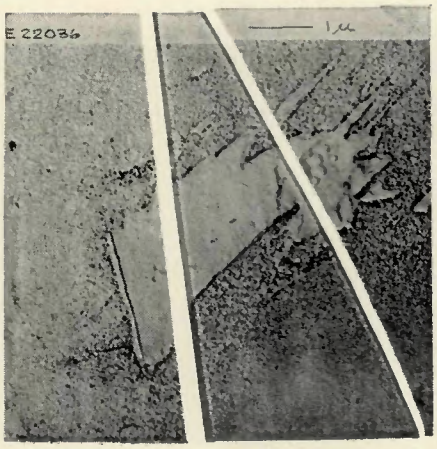

Fig. 16—Specimen 2-6, 2-7 (250 Grade 18 Ni) showing Ti (C,N) precipite at boundary of austenite island

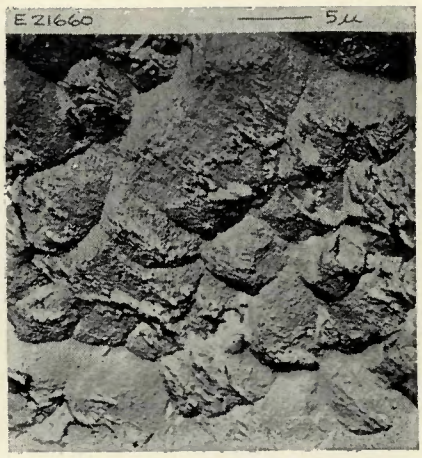

Fig. 17—Specimen 36 (300 Grade 18 Ni) fractured surface showing effect of titanium-type precipitates on mode of cracking

18 Ni grade weldments revealed a rod-like and angular precipitate. These precipitates are indirectly identified to be Ti compounds by their color and by similar shape precipitates being reported as Ti (C, N). [6]The segregation of this precipitate at the austenite martensite interface can reduce the mechanical strength and does affect the mode of cracking—Figs. 15–17.

The Role of Hydrogen in Stress Corrosion Cracking of 18 Ni Maraging Steel Weldments

An optical method for detecting the emanation and distribution of hydrogen in maraging steels was developed based on the reaction of hydrogen with a rare earth metal to form a metal hydride.[7] Neodymium film is evaporated on a polished and etched cross-section of a 250 grade 18 Ni weldment. The sample is heated to evolve the hydrogen from the steel surface and to speed the reaction of the emitted hydrogen with the neodymium metal overlay. The neodymium film is optically transparent so that the microstructure can be related to the black neodymium hydride reaction sites.

An 18 Ni maraging steel weldment was charged with H_2. Examination of the maraging steel microstructure, in relation to the hydrogen, revealed hydrogen emanating from the austenite islands and along the martensite subgrain boundaries— Fig. 18.

This sample was previously evaporated with a Nd film and heated before being artificially charged with hydrogen. Hydrogen was observed to emanate from the austenite island (Fig. 19) with only a few large H_2 reaction sites. Another hydrogen test was performed on the same specimen after repolishing and cathodically charging with H_2 to reveal additional emittance characteristics. Hydrogen was observed to emanate in a preferred mode associated with unidentified martensite crystallographic directions—Fig. 20. Similar martensite laths were also observed forming in the H_2 cathodically charged austenite islands—Fig. 21. These strain induced martensite transformations could be produced by a combination of hydrogen and stress interaction.

The hydrogen reaction sites were further resolved by examination with a scanning electron microscope (SEM). An SEM micrograph revealed the cluster

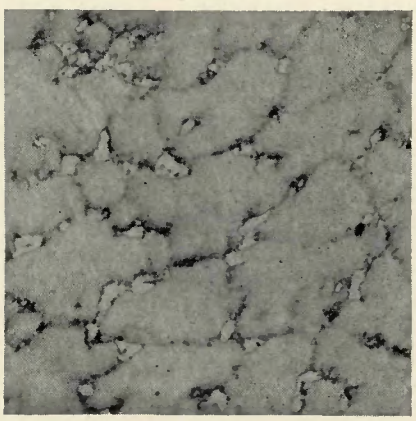

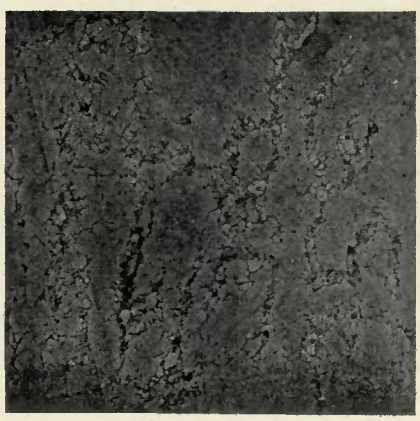

Fig. 18—Specimen 2-6, 2-7 (250 Grade 18 Ni) showing NdH_2 reaction sites. X885 (reduced 38% on reproduction)

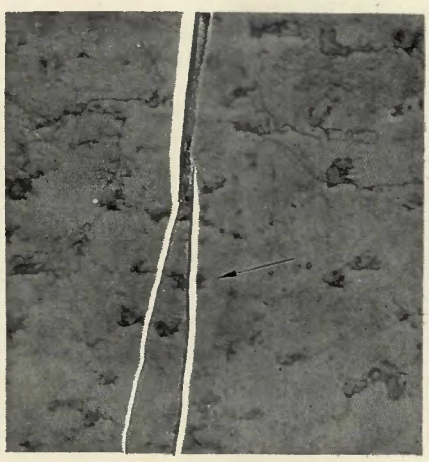

Fig. 19—Specimen 2-6, 2-7 (250 Grade 18 Ni) with evaporated Nd film showing NdH_2 reaction site in austenite island. X940 (reduced 33% on reproduction)

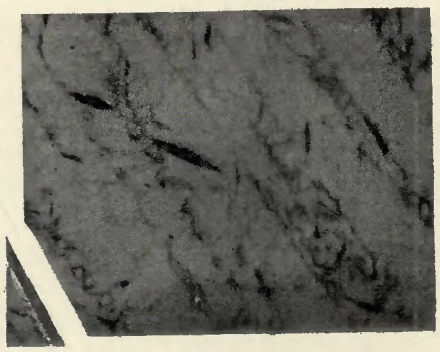

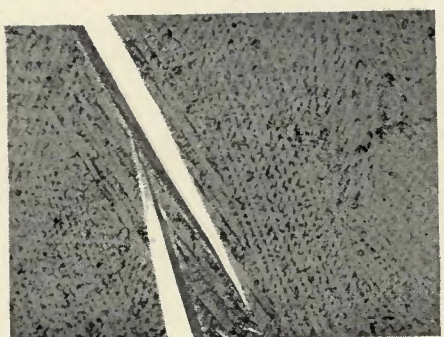

Fig. 20—Specimen 2-6, 2-7 (250 Grade 18 Ni) showing hydrogen emanation and distribution along crystallographic directions

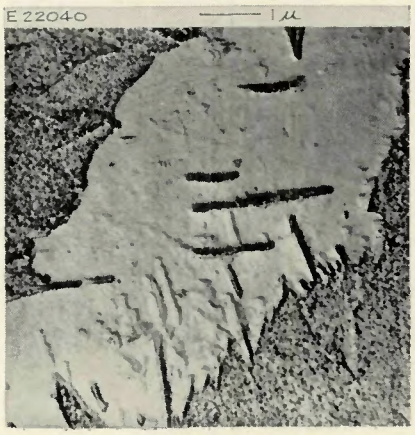

Fig. 21—Upheaval of austenite polished surface by strain-induced martensite transformation in H_2 cathodically charged maraging stel weldment

of NdH_2 reaction sites over the austenite island. Other individual reaction sites were observed bunched up toward the austenite islands along preferred martensite subgrain boundary lines—Fig. 22. These martensite crystallographic directions could be related to the herringbone pattern observed on the quasi-cleavage fracture surfaces discussed in the fractography section. Indirect evidence of this relationship is the 110 deg angle between the intersecting crystallographic directions found in austenite, martensite, and on the fractured surfaces.

The specimen was repolished and etched by the two-step etching process. Neodymium was deposited on half of the specimen, and the specimen was then heated at 300° F (149° C) for $1^1/_2$ hr in vacuum and then removed; the optical resolution was excellent—Fig. 18.

A Zeiss surface interferometer was used to measure the Nd film thickness which was 2,825 ± 125A.

Theoretical Calculation of Hydrogen Emission

A theoretical calculation of hydrogen emanating from an austenite island and from martensite subgrains was estimated, based on a cylinder shape. The facets have the average diameter of the NdH_2 reaction sites observed in the photographs. The length of the cylinder for the steel specimen was based on diffusion length x_i calculated by the familiar approximation that $x_i = Dt$ where D is the diffusion coefficient and t is the time.[8] The length of the NdH_2 cylinder was assumed to be an average measured thickness of 2,800 Å. An average hydrogen content of 6 ppm for the 250 grade 18 Ni maraging steel after H_2 charging was assumed to be reasonable.[9] H_2 diffusion time, t, was 1 hr at 300° F (149° C). Diffusion coefficient values were taken from published data.[10]

The entry, movement, and diffusion of hydrogen in the 250 grade 18 Ni maraging steel weldments is not fully understood. Theoretical calculations on the amount of hydrogen expected to be emitted from the austenite and martensite sites by diffusion can be made and then compared to the theoretical calculated amount of hydrogen reacted with the neodymium film to form the compound NdH_2.

The H_2-Nd reaction site is assumed to be a cylinder of austenite with an overlay of an evaporated Nd film which converts completely to NdH_2—Fig. 23. The H_2 emits from the austenite assuming a concentration of 6 ppm. This concentration of hydrogen is reasonably expected for H_2 cathodically charged into martensite.

For these calculations the density values used were $\rho(Fe) = 7.87$ gm/cc

Fig. 22—SEM micrographs of NdH_2 reaction sites in 250 Grade 18 Ni maraging steel weldment. X10,000 (reduced 41% on reproduction)

$+ \rho(Nd) = 6.8$ gm/cc. A sample calculation is given as follows:

Bulk diffusion of hydrogen from austenite at 300° F (149° C) for 1 hr:[6]

$$X_i^2 = Dt$$

$$X_i^2 = \sqrt{Dt}$$

$$= \sqrt{(1 \times 10^{-8})(3.6 \times 10^{3})}$$

$$= \sqrt{3.6 \times 10^{-5}}$$

$$= 0.6 \times 10^{-3} \text{ cm}$$

Now the amount of weight, W_{Fe}, in the diffusion zone can be calculated, where A is area of cylinder face and V is volume of austenite:

$$W_{Fe} = \rho V = (\rho)(Xi)(A)$$

$$= (7.87)(0.6 \times 10^{-3})(3.14 \times 10^{-8})$$

Table 5—Theoretical Calculations of H_2 Emitted in One Hour at 300° F

Case no.	Diffusion coefficient, cm^2/sec	Area A,[a] cm^2	Diffusion length X_i cm	Weight Fe, gm	Weight[b] emitted H_2, gm	Weight H_2 reacted to form NdH_2, gm	H_2 removed from Fe, ppm
1a	$D_\lambda = 1 \times 10^{-8}$ bulk	3.14×10^{-6}	0.6×10^{-3}	1.48×10^{-11}	8.8×10^{-17}	1.82×10^{-13}	12,400
1b	$D_\lambda = 1 \times 10^{-6}$ G. B.	3.14×10^{-6}	0.19	4.69×10^{-8}	2.79×10^{-13}	1.82×10^{-13}	3.9
2a	$D_\alpha = 5 \times 10^{-5}$ bulk	3.1×10^{-10}	0.42	1.02×10^{-8}	6.12×10^{-14}	1.97×10^{-15}	0.2
2b	$D_\alpha = 5 \times 10^{-3}$ G. B.	3.1×10^{-10}	2.24	5.5×10^{-7}	3.3×10^{-12}	1.97×10^{-15}	0.03

[a] Based on ideal diameter measured from SEM photograph.
[b] Based on 6 ppm H_2.

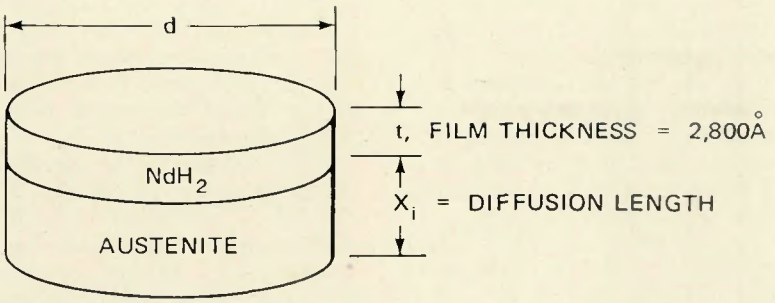

Fig. 23—Model of H_2 reaction site

$$= 1.48 \times 10^{-11} \text{ gm}$$

Assume 6 ppm H_2 in austenite, then the weight of hydrogen emitted W_{H2} can be calculated.

$$W_{H2} = (6 \times 10^{-6})(W_{Fe})$$
$$= (6 \times 10^{-6})(1.48 \times 10^{-11})$$
$$= 8.8 \times 10^{-17} \text{ gm } (H_2 \text{ emitted})$$

Now the weight of neodymium W_{Nd} can be calculated where T is Nd film thickness.

$$W_{Nd} = \rho V = \rho TA$$
$$= (6.8)(2800 \times 10^{-8})(3.14 \times 10^{-8})$$
$$= 5.45 \times 10^{-12} \text{ gm}$$

The weight of hydrogen reacted with Nd can be calculated by the following equation where molecular weight is *mw:*

$$W_{H2} = \frac{W_{Nd}}{mw\,(Nd)} \times mw\,(H_2)$$

$$W = 5.45 \times 10^{-12}\left(\frac{2}{60}\right)$$
$$= 1.82 \times 10^{-13} \text{ gm } (H_2 \text{ reacted with Nd})$$

$$W_{H2} = \frac{1.82 \times 10^{-13} \times 10^{6}}{1.48 \times 10^{-11} \times 10^{6}}$$
$$= 1.24 \times 10^{-2} \text{ or equivalent to 12,400 ppm } H_2 \text{ emitted.}$$

The theoretical calculations of hydrogen emitted in 1 hr are given in Table 5. By comparing the amount of hydrogen that can be emitted by diffusion with that detected by the hydrogen reacted to form NdH_2, the following interpretations are made:

Case No. 1a. Hydrogen emission by bulk diffusion through austenite cannot account for the amount of hydrogen detected by the Nd hydrogen detector. Hydrogen diffusion from traps can give the right order of magnitude of H_2. Compare W_{H2}, $D\gamma_{Bulk}$ values (columns 4 and 5, Table 5).

Case No. 1b. Grain boundary diffusion of hydrogen in austenite is sufficient to account for the H_2 detected. Compare W_{H2}, $D\gamma_{GB}$ values (columns 4 and 5, Table 5).

Cases 2a and 2b. Both bulk and grain boundary diffusion for martensite can account for the H_2 detected. If H_2 diffusion was due to a one-atmosphere source of hydrogen, the values calculated would be greater than the H_2 detected; therefore, when favorable test conditions exist, it is possible to distinguish between emission of hydrogen either by molecular hydrogen coming from traps or by interstitial hydrogen. The last column in Table 5 indicates the hydrogen detected in terms of ppm removed from the H_2 reaction site model—Fig. 23. The higher amount of hydrogen emanating from the austenite phase is reasonably expected since the solubility of hydrogen is greater in austenite than in iron.

The solubility of hydrogen in austenite at its transition temperature is reported to be 4.5 ppm H_2 and 2 ppm for alpha iron at 149° C (300° F).

The hydrogen emanating from the austenite islands cannot be accounted for by bulk diffusion because the emittance is too small. However, it can be accounted for by grain boundary diffusion atomic hydrogen or by permeation of molecular H_2 from traps in the bulk austenite.

If one uses the extrapolated permeation rate of 5×10^{-7} cc/cm²/hr at 300° F (149° C) for a 1 mm thick austenite membrane with an upstream hydrogen pressure af 1 atm, it is the same order of magnitude as the calculated 2.88×10^{-8} cc/cm²/hr detected by the Nd hydrogen detector. The results could be interpreted as evidence of both interstitial and molecular hydrogen movement in austenite.

In the case of hydrogen emanation from the martensite sub-boundaries, the emission rate is calculated to be 2.86×10^{-10} cc/cm²/hr which is much lower than the extrapolated permeation rate value for α Fe of 10^{-3} cc/cm²/hr. The hydrogen emanating from the martensite is principally contributed by interstitial hydrogen movement. Furthermore, the hydrogen detected by the NdH_2 detector does not correlate with the hydrogen emitted by grain boundary diffusion. This would mean the hydrogen is principally moving out of the bulk martensite.

There are two situations where the critical hydrogen concentration and stress would be very favorable for initiation of stress corrosion cracking

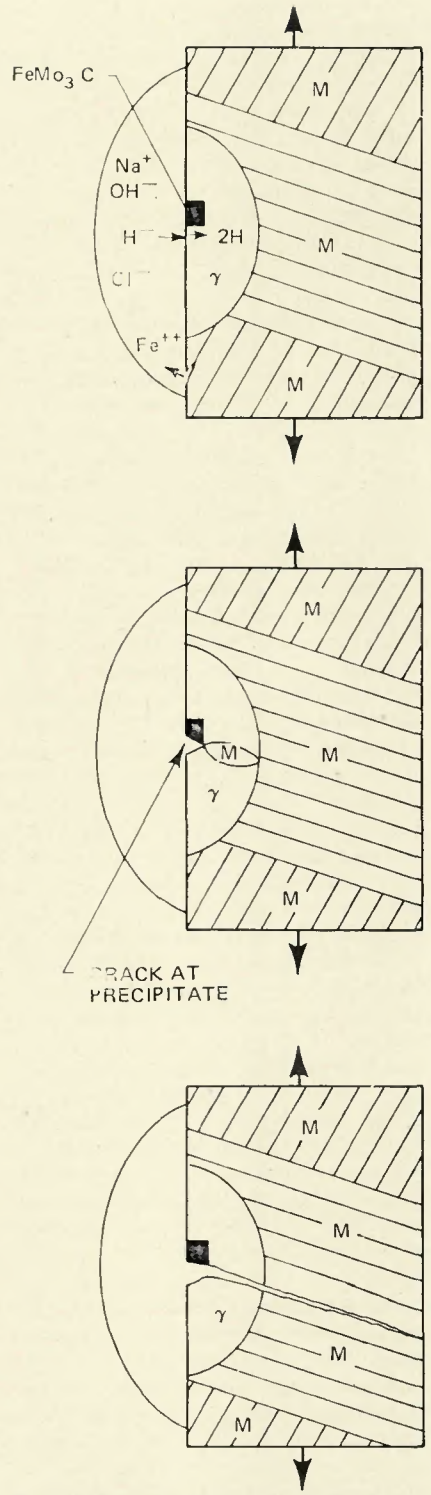

Fig. 24—Model of proposed stress corrosion cracking mechanism of 18 Ni maraging steel weldment. A (top)—electrochemical attack produces hydrogen which enters austenite; B (center)—stress is sufficient to form crack at precipitate—austenite transforms to martensite which is embrittled by hydrogen originally in the austenite; C (bottom)—cracks propagates along preferred orientation into the martensite matrix

of the maraging steel weldments. A stress is concentration at one of the observed preferred crystallographic interfaces (along subgrain boundaries) of the martensite. The martensite is strained and the movement of interstitial hydrogen by diffusion to this local area results in hydrogen embrittlement.[10] When a stress concentration situation occurs, a high H_2-containing austenite island is strained and transforms to martensite. The movement of the hydrogen from the martensite to the remaining austenite embrittles the transforming martensite, particularly at the points of the feathery needle-like phase. This propagates into the martensite matrix where it initiates martensite cleavage along the similar crystallographic direction observed both in transformed martensite, in austenite, and martensite subgrain boundaries.

Obviously, the reverse situation can occur where movement of the hydrogen embrittles the strained matrix martensite. It cracks and propagates into the austenite causing the austenite to transform to martensite. The hydrogen solubility in martensite is lower than for austenite and the hydrogen must diffuse.

Three electochemical electrodes which can provide favorable cathodic hydrogen reduction are: γ-metal carbide; α-Ti (C,N); and γ-α. These phases form electrochemical cells with austenite or the martensite matrix causing enough hydrogen to be generated at the cathode to embrittle the austenite or martensite. Iron is the principal oxidized element and hydrogen the reduced element.[11]

A model of a proposed stress corrosion mechanism of 18 Ni maraging steel weldment is illustrated in Fig. 24. An electrochemical cell is formed on the surface of the maraging steel weldment. Iron goes into solution and hydrogen is introduced into the austenite.[11]

A crack at the $FeMo_3C$ or other precipitate is formed in the austenite when stress is applied. The stress intensity increases ahead of the crack in the austenite. When a critical stress is reached, transformation of the austenite to martensite is initiated along preferred orientations. The hydrogen originally in the untransformed austenite now embrittles the strained martensite which cleaves and the crack prefers to propagate into the martensite matrix along a matching martensite similarly oriented. The process is repeated until failure occurs.

The hydrogen embrittlement process is also applicable to delayed failure of the 18 Ni maraging steel in pentaborane. If pentaborane is decomposed by a catalytic or chemical reaction, hydrogen is released.[12] The τ-Ti_2S could be a suitable catalytic poison. The atomic hydrogen prefers to enter the austenite. When sufficient strain is introduced into the austenite it transforms to hydrogen embrittled martensite.

Recommendations for Prevention of Stress Corrosion Cracking of 18 Ni Maraging Steel Weldments

It is recommended that the chemistry of the austenite be modified to raise the *Ms* temperature to provide complete transformation of the austenite to martensite during welding or to lower the *Ms* temperature to stabilize the austenite. This would require developing a welding rod with a suitable chemical composition.

It should also be noted that martensite reverting to austenite in the heat affected zone is another possible H_2 sensitive phase. The reverted austenite could be transformed to martensite in a similar manner as the retained austenite.

Conclusions

The characteristics exhibited by stress corrosion cracking of 18 Ni maraging steel weldments identified by electron microscopy, scanning electron microscopy, electron diffraction, H_2 emission and distribution, and electrochemical data are presented as evidence that hydrogen embrittlement plays a major role in the failure mechanism.

Delayed failure of the 18 Ni maraging steel weldment in air is associated with an electrochemical mechanism, where cathodic hydrogen reaction is the source for the hydrogen embrittlement to occur. Delayed failure of the weldments in pentaborane has not been identified as chemical or electrochemical at this time.

The retained austenite in the weldment is primarily responsible for the stress corrosion susceptibility. It is postulated that hydrogen is built up in the retained austenite. It has been shown that the combination of local stress and hydrogen is necessary to initiate transformation of the retained austenite into an H_2 embrittled martensite along preferred orientations.

It is recommended that the chemistry of the austenite be modified to alter the M_s and M_f temperature resulting in either a stable austenite or a complete transformation of the austenite to martensite during welding. Theoretical calculations of M_s and M_f indicated that this could be accomplished by modifying the composition of the welding rod to attain the desired results.

Acknowledgment

This work was sponsored by Independent Research and Development Funding at McDonnell Douglas Astronautics Company.

References

1. Taketani, H., "Stress Corrosion Susceptibility of Welds in Maraging Steel and Cryoform 301 Stainless Steel," DAC Report 62999, Aug. 1969, pp. 1-31.

2. Rawe, R. A., "Fracture Mechanics in Design for Safe Life," DAC Report 4880, March 1969, pp. 1-42.

3. Reisdorf, B. G., and Salmon Cox, P. H., "Investigation of Thermal Embrittlement in 18 Ni (250) Maraging Steel," 3rd Quarterly Report AF 33 (615)-278, May 1966, pp. 1-24.

4. Streicher, M. A., "Effects of Heat Treatment Composition and Microstructure on Corrosion of 18 Ni-Ti Stainless Steels in Acids," Corrosion 20, 57t (1964), pp. 57t-72t.

5. Floreen, S., "The Physical Matallurgy of Maraging Steels," Technical Paper 563-OP. International Nickel Co., Inc. Suffern, N.Y., pp. 1-40.

6. Reisdorf, B. G., Birkle, A. J., and Salmon Cox, P. H., "Kinetics and Mechanisms of the Strengthening of Maraging Steels," Eighth Quarterly Report: AF 33 (657)—11149 April 15, 1965, pp. 1-50.

7. Korst, W. L., "Studies of the Rare Earth Hydrides," PHD Thesis, Chem, C 56 K84; University of Southern Calif. L.A., June 1956, p. 190.

8. Darken, L. S., and Gurry, R. W., "Physical Chemistry of Metals," McGraw-Hill (1953), p. 444.

9. Gray, H. R., and Troiano, A. R., "How Hydrogen Affects Maraging Steel," Metal Progress, April 1964, p. 75.

10. "Hydrogen Movement in Steel Entry. Diffusion and Elimination," DMIC Report 219, p. 40.

11. Toy, S. M., "Polarization of Strained AISI 4340 Steel in Oxygenated NaCl Solutions," Corrosion 22, 238, (1966), pp. 229-237.

12. Cloyd, D. R., and Murphy, W. J., "Handling Hazardous Materials," NASA SP-5032, Sept. 1965, pp. 29-41.